

Single-particle electronic spectra of quantum rings: A comparative study

J. Simonin and C. R. Proetto

Centro Atómico Bariloche and Instituto Balseiro, 8400 S.C. de Bariloche, Río Negro, Argentina

Z. Barticevic and G. Fuster

Departamento de Física, Universidad Técnica Federico Santa María, Casilla 110-V, Valparaíso, Chile

(Received 23 June 2004; published 5 November 2004)

The single-particle electronic spectra of semiconductor self-assembled quantum rings are theoretically analyzed. We studied two different models for the lateral confining potential: the displaced parabola (Hill) and the centrifugal-like core (Volcano). The corresponding energy levels are systematically analyzed as a function both of the ring radius, and external magnetic fields perpendicular to the ring plane. The one-electron ground state of the Hill potential presents an absolute minimum when studied as a function of the ring radius. Numerically exact and approximate solutions are compared for the case of the Hill ring. Each one of the two ring models leads to a characteristic level crossing pattern in the presence of a perpendicular magnetic field, which can be used to identify which of both models is more suitable to fit one-electron spectroscopic data. The electronic spectrum of elliptical Hill rings, with broken azimuthal symmetry, is also presented. It is found that the Hill confinement potential provides a more suitable theoretical description of nanoscopic semiconductor self-assembled rings than the Volcano confinement.

DOI: 10.1103/PhysRevB.70.205305

PACS number(s): 78.67.Bf, 73.21.-b, 73.40.Rw, 78.66.Fd

I. INTRODUCTION

The ring geometry has long been a useful tool for the observation of interference effects in electron trajectories, i.e., quantum effects.¹ Submicron-diameter man-made metallic rings have been available for a while and a large number of ground-breaking experiments have been made on them, studying their magnetic and transport properties.² These studies have been carried out in the mesoscopic range, where scattering still influences the phase coherent transport and a large (macroscopic) number of electrons are present.

Recently, semiconductor ring samples in the quantum confined regime have been fabricated on AlGaAs—GaAs heterostructures containing a two-dimensional electron gas (2DEG).^{3,4} Using an atomic force microscope to apply a voltage between the tip and the 2DEG, the electron gas can be permanently depleted below the biased regions. This allows the “writing” of heterostructures at the scale of hundreds of nanometers, resulting in rings with about 200 electrons. Through magnetotransport experiments in the Coulomb blockade regime on these rings many microscopic features of the energy spectra were obtained, in spite of the still large number of electrons filling the available quantum-ring states.

More recently, but using a different fabrication procedure, two-dimensional (2D) self-assembled InAs semiconductor rings have been obtained in the nanoscopic range, providing spectroscopic data in the scatter-free, few-electrons limit.⁵ Spectroscopic techniques were used to investigate both the ground state and the excitations of these rings, by changing the number of electrons and by application of external (typically magnetic) fields.⁶

Although a detailed study of the electron-electron interaction in the two-, three-, and few-electron cases will be the most interesting theoretical features of these rings, the analysis of the one-body confinement is a necessary first step. The

present contribution aims at analyzing the electronic structure of single occupied rings, and by comparison with experiments at determining which of the available theoretical models used to represent the ring confinement is more suitable. The main conclusion of the present work is that the displaced parabola is a better theoretical model for the lateral confinement of semiconductor self-assembled rings than the centrifugal-like core potential.

The rest of the paper is organized as follows. In Sec. II we introduce the analyzed ring-confining potentials and explain the analytical and numerical methods that we use for the solution of the one-particle problem. In Sec. III we provide the results in three different situations: zero magnetic field, nonzero magnetic field, and rings with broken azimuthal symmetry. In Sec. IV we provide a fitting to a particular set of experimental data on self-assembled semiconductor quantum rings, using the Hill confinement potential. Section V presents the conclusions. We include also an Appendix with some important remarks on ladder operators.

II. METHOD AND ANALYZED POTENTIALS

In the semiconductor ring samples discussed in the Introduction, the movement of the electrons along the growth direction (the z axis) is “frozen” in the ground state of the strong epitaxial potential which builds up along this direction. Therefore, one is left to deal with the dynamics of the electrons in the xy plane: the 2D electron gas. The lateral confining potentials are typically much smaller than the epitaxial potential, and experiments usually involve transitions between lateral states.

In order to resolve the low-energy properties of nonanalytically solvable ring potentials we use a standard method: We evaluate the matrix elements of the given potential on the basis of the 2D-quantum Dot potential, i.e., the 2D-harmonic

oscillator.⁷ We then diagonalize numerically the corresponding matrix Hamiltonian, using a basis as large as necessary to obtain a given accuracy. By default we use a 256 states basis for each m subspace, this basis can be doubled as many times as needed. The allowed orbitals for the ring potential are thus obtained as a linear combination of the Dot orbitals.

For the quantum Dot potential $\frac{1}{2}k\rho^2$, in the presence of a magnetic field B perpendicular to the plane of the dot (with the vector potential in the symmetric gauge $\mathbf{A}=\frac{1}{2}B[y, -x, 0]$) the electron (charge $-e$, mass m_e^*) eigenfunctions in the polar coordinates (ρ, φ) real-space representation are classified by their radial $n=0, 1, 2, \dots$, and azimuthal $m=0, \pm 1, \pm 2, \dots$, quantum numbers, and are given by

$$\Psi_{n,m}^D = \frac{1}{\sqrt{\pi}\lambda_\omega} (p_{|m|}^n)^{1/2} e^{im\varphi} \chi^{|m|/2} e^{-\chi/2} L_n^{|m|}(\chi), \quad (1)$$

with eigenvalues

$$E_{n,m}^D = \hbar\omega_o[(2n+1+|m|)\sqrt{1+b^2}-mb], \quad (2)$$

the well-known Fock-Darwin spectrum.^{8,9}

In these equations $\omega_o = \sqrt{k/m_e^*}$ is the characteristic Dot frequency of the lateral confinement, b is the ratio of the cyclotronic frequency to twice the Dot frequency ($b = \omega_B/2\omega_o$, $\omega_B = eB/m_e^*c$). The perpendicular magnetic field also renormalizes the frequency $\omega = \omega_o\sqrt{1+b^2}$ and the characteristic length $\lambda_\omega = \lambda_o\sqrt{\omega_o/\omega} = \lambda_o/(1+b^2)^{1/4}$, where $\lambda_o \equiv \sqrt{\hbar/m_e^*\omega_o}$ is the zero-field characteristic length of the Dot potential. In the orbital equation, $L_n^{|m|}$ are the generalized Laguerre polynomials, $p_{|m|}^n \equiv n!/(n+|m|)!$ and $\chi = (\rho/\lambda_\omega)^2$. These orbitals depend on the magnetic field through the renormalized length λ_ω .

We use these results of the Dot potential to set the energy, length, and magnetic field scales for the rest of the paper; they are, respectively, $\hbar\omega_o$, λ_o , and $2cm_e^*\omega_o/e = \Phi_o/\pi\lambda_o^2$. Note that, in these units, the “renormalized” magnetic field b can be interpreted as the number of flux quanta $\Phi_o = ch/e$ threading a circle of radius λ_o ($b = B\pi\lambda_o^2/\Phi_o$). In the self-assembled rings for which this study is intended,⁵ $\hbar\omega_o$ is of the order of 10 meV, $\lambda_o \sim 100$ Å (ten nanometers), and fields of several tesla can be applied to the samples, which implies values of b up to a few units.

These nm -Dot orbitals can also be expressed in different representations¹⁰ (see, for example, the Appendix), and the matrix elements of nonanalytically solvable potentials can usually be found easily. Matrix elements of many-body effects (like the Coulomb interaction) can also be explicitly calculated.¹¹

We compare here two possible ringlike confining potentials: the displaced parabola (“Hill”)⁷

$$V_H(\rho) = \frac{1}{2}(\rho - \rho_o)^2, \quad (3)$$

and the “centrifugal core” (“Volcano”)^{12,13}

$$V_V(\rho) = \frac{1}{2}(\rho - \rho_o^2/\rho)^2. \quad (4)$$

As quoted above, energies are in units $\hbar\omega_o$ and lengths in units of λ_o . The position of the minimum of the potential (ρ_o) is defined as the radius of the ring. Both the Hill and the Volcano potentials reduce to the Dot in the $\rho_o \rightarrow 0$ limit.

The Volcano potential is an exactly solvable model:¹² The repulsive core [$\sim(\rho_o^2/\rho)^2$] adds to the centrifugal potential [$\sim(m/\rho)^2$] to give an “effective” angular momentum $M = \sqrt{m^2 + \rho_o^4}$, which has a finite value even for zero angular-momentum states, $M = \rho_o^2$ for $m=0$. The eigenstates of the Volcano potential are also given by Eq. (1), but with $|m|$ replaced by M everywhere. These Volcano orbitals depend on ρ_o through M , the renormalized “angular momentum.” This introduces the effect of the repulsive core of the Volcano in their radial distribution. Note the ρ^M factor: These orbitals vanish at the origin even for $m=0$.

The corresponding energies are

$$E_{n,m}^V = [(2n+1+M)\sqrt{1+b^2} - mb - \rho_o^2] \quad (5)$$

very similar to the Fock-Darwin expression [Eq. (2)]. There is, however, an important difference: The crossing of energy levels as a function of the applied magnetic field is already embodied in it. This is a typical feature of multiple connected geometries, such as rings.

The eigenvalues and eigenfunctions of the Hill potential should be obtained numerically. We do this in the following sections, where their properties are also compared with those of the Volcano potential. For large values of ρ_o ($\gg 1$, near the 2D-wire limit) we use the modified basis of an 1D-harmonic oscillator, best suited for this situation.¹⁴

III. RESULTS

A. Zero magnetic field

First, let us analyze the energy levels of the Hill and Volcano potentials as a function of ρ_o at zero applied magnetic field. Rotational symmetry is preserved, and thus the matrix for the ring Hamiltonian is block diagonal, with one block for each value of m .

Figure 1 shows that for $\rho_o \gg 1$ the eigenvalues of both potentials tend to those of a straight 2D-wire, i.e., a $(n+1/2)$ term corresponding to the 1D parabolic potential representing the confinement across the wire plus a free particle band for the dynamics along the wire. Each band corresponds to a given value of n , and all values of m . In this limit the effective frequency for the Volcano is twice the Hill frequency: expanded around ρ_o the Volcano potential is four times stronger than the Hill potential,

$$(\rho - \rho_o^2/\rho)^2 = 4(\rho - \rho_o)^2 + O(\rho - \rho_o)^3,$$

for $\rho_o \neq 0$; and accordingly, the limiting value for the confinement frequency across the wire for the Volcano case is twice the corresponding Hill one.

The ground state (GS) of the Volcano (and all its $m=0$ states) does not depend on ρ_o . This is not the case for the Hill potential: The lowest eigenvalue ($n=0, m=0$) goes from 1 to $1/2$ as ρ_o increases, with an absolute minimum ($E_{0,0}^H \approx 0.431$) at $\rho_o \approx 1.523$. A similar behavior can be observed for all the $m=0$ eigenvalues of the Hill potential, although

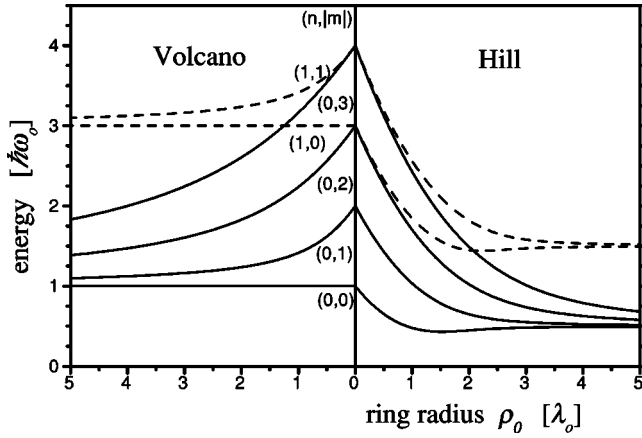


FIG. 1. Lowest lying energy levels for the Volcano (left) and Hill (right) ring potentials, as a function of the ring radius ρ_o . Full lines: $n=0$, m levels; dashed lines: $n=1$, m levels. The degeneracy for the Dot ($\rho_o=0$) energy levels with the same value of $2n+|m|$ is broken in the ring ($\rho_o \neq 0$) case, which only conserves the $\pm m$ degeneracy. The ground state of the Hill potential displays an absolute minimum of $E_{0,0}^H=0.4315$ at $\rho_o=1.523$.

the minimum becomes less pronounced as m increases. As soon as ρ_o increases from zero, the leading effect on the orbitals of the Hill potential is equivalent to that of an effective wider (softer) dot. The $m=0$ orbitals (for the different values of n) take full advantage of this situation, and the corresponding energies have an absolute minimum as a function of ρ_o . For the $m \neq 0$ orbitals, as well as for the Volcano potential, the centrifugal term of the Hamiltonian precludes this effect, and the corresponding energies monotonically decrease from their values at $\rho_o=0$ (Dot limit) to their values at $\rho_o \gg 1$ (2D-wire limit).

Different approaches can be used to further analyze these minima. In order to check also the power of the numerical method we first use a minimal Dot basis to evaluate the GS of the Hill potential for values of ρ_o near zero: we just take the two first Dot eigenfunctions of the corresponding Hilbert subspace ($m=0$)

$$|1\rangle = \Psi_{0,0}^D = e^{-\rho^2/2}/\sqrt{\pi}, \quad (6a)$$

$$|2\rangle = \Psi_{1,0}^D = e^{-\rho^2/2}(1-\rho^2)/\sqrt{\pi}. \quad (6b)$$

The matrix elements of the Hill Hamiltonian (H_H) in the Dot basis, in a given m subspace, are

$$\langle n|H_H|n'\rangle_D = \delta_{nn'}(E_{nm}^D + \rho_o^2/2) - \rho_o \langle n|\rho|n'\rangle_D. \quad (7)$$

In other words, the matrix elements of the Hill Hamiltonian in the Dot basis are diagonal in m , but the second term on the right-hand side of Eq. (7) mixes the Dot eigenstates with different radial quantum numbers.

For the present 2×2 Hilbert subspace matrix, the elements are:

$$\langle 1|H_H|1\rangle = 1 - \frac{\sqrt{\pi}}{2}\rho_o + \frac{\rho_o^2}{2}, \quad (8a)$$

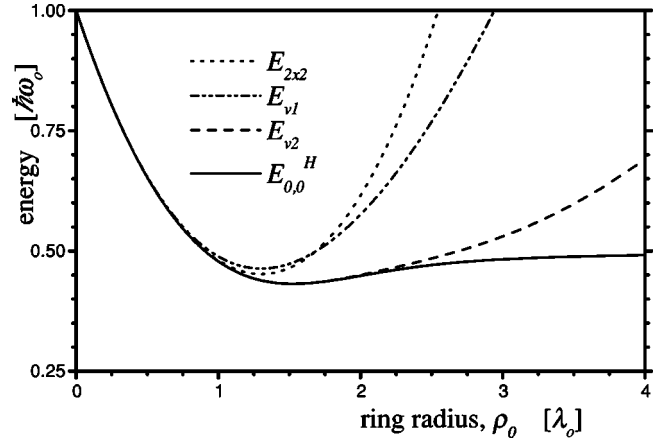


FIG. 2. Energy of the GS Hill orbital as a function of ρ_o . $E_{0,0}^H$ is the exact result; $E_{2 \times 2}$ is the energy that results from a minimal basis expansion. E_{v1} and E_{v2} are variational solutions.

$$\langle 2|H_H|2\rangle = 3 - \frac{7\sqrt{\pi}}{8}\rho_o + \frac{\rho_o^2}{2}, \quad (8b)$$

$$\langle 1|H_H|2\rangle = \langle 2|H_H|1\rangle = \frac{\sqrt{\pi}}{4}\rho_o. \quad (8c)$$

This matrix can be easily diagonalized analytically; the lowest eigenvalue, expanded around $\rho_o=0$ for clarity, reads

$$E_{2 \times 2} = 1 - \frac{\sqrt{\pi}}{2}\rho_o + \left(1 - \frac{\pi}{16}\right)\frac{\rho_o^2}{2} + \dots, \quad (9)$$

showing explicitly the initial negative slope towards the minimum. The full expression for the lowest energy level of this minimal Hilbert space is plotted in Fig. 2, with a dotted line. This eigenvalue has a minimum at $\rho_o=1.301$, with $E_{2 \times 2}=0.452$, quite close to the real values, despite the fact that we use just two Dot orbitals as the expanding basis.

We use now variational wave functions in order to gain more insight into the nature of this absolute minimum in the energy spectrum. First, we use a very simple ansatz: a modified Dot (0,0) eigenfunction,

$$\Psi_{v1} = e^{-\rho^2/2\beta^2}/\sqrt{\pi}\beta, \quad (10)$$

where the variational parameter β allows the wave function to be more (less) extended than the original Dot orbital if $\beta > 1$ ($\beta < 1$). We evaluate the expectation value of the Hill Hamiltonian for this state

$$E_{v1}(\beta) = (1 + \rho_o^2\beta^2 + \beta^4 - \rho_o\beta^3\sqrt{\pi})/2\beta^2. \quad (11)$$

Minimizing it with respect to β we obtain the value of $\beta(=1 + \rho_o\sqrt{\pi}/8 + 3\pi\rho_o^2/128 + \dots)$ that optimizes this energy as a function of ρ_o . The main effect is that of a softer (or wider) dot, i.e., $\beta \geq 1$, thus $\lambda_{\text{effc}} = \beta\lambda_o \geq \lambda_o$. From these equations we can obtain an approximation to the absolute minimum: $E_{v1} \cong 0.463$ at $\rho_o \cong 1.302$, close to the exact result.

With a slightly more refined variational ansatz

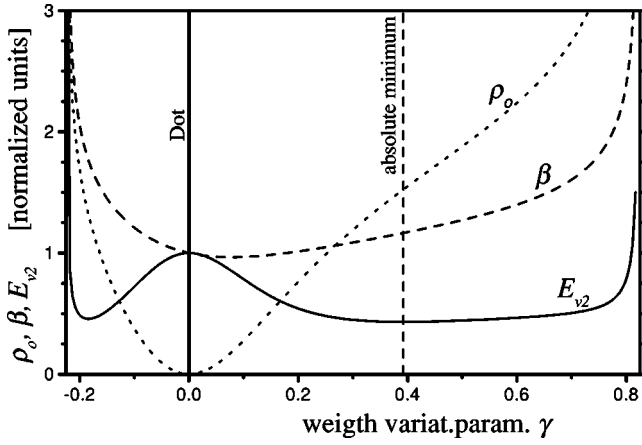


FIG. 3. The parametric solution for Ψ_{v2} : E_{v2} , ρ_o , and β as a function of γ . Note that the $\gamma=0$ point corresponds to the exact Dot GS: $\gamma=0$, $\beta=1$, $\rho_o=0$ and $E_{v2}=1$.

$$\Psi_{v2} = e^{-\rho^2/2\beta^2} [\sqrt{1-\gamma^2} + \gamma(\rho^2/\beta^2 - 1)] / \sqrt{\pi}\beta, \quad (12)$$

which is just a linear combination of the first two Dot eigenfunctions, weighted with the variational parameter γ , and each one renormalized by β , which plays the same role as in Ψ_{v1} . Nearly exact results are obtained for $\rho_o \lesssim 2$ (dashed line in Fig. 2).

The calculation for Ψ_{v2} is similar to the one for Ψ_{v1} , but it is a little more complex due to the presence of two variational parameters. Instead of explicit equations for the optimal values β and γ (and then E_{v2}) as functions of ρ_o , it unfolds in a nice analytical parametric solution: Given γ , the corresponding optimal $\beta(\gamma)$ is determined, then $\rho_o[\beta(\gamma), \gamma]$, and then $E_{v2}(\rho_o[\beta(\gamma), \gamma], \beta(\gamma), \gamma)$. These parametric solutions (β, ρ_o, E_{v2}) are shown in Fig. 3. as a function of γ . The optimal values of β and γ at the minimum of the spectrum are 1.165 and 0.392, respectively.

Although small, the electronic energy gained in the growing process by setting the ring radius at values near this minimum could help to stabilize these self-assembled rings.¹⁵ In fact, the radii of the rings of Ref. 5 are near this value. Coulomb energies can also be expected to decrease for wider orbitals, favoring the transition from dots to rings.

B. Nonzero magnetic fields

In the presence of an applied magnetic field, perpendicular to the plane of the rings, the typical level crossing of multiple connected geometries as a function of the “trapped” flux appears. In Fig. 4 we show the Hill spectrum at $\rho_o = 1.523 (= \rho_{\min})$ as a function of the applied magnetic field. The starting point of the spectrum ($b=0$, but $\rho_o = \rho_{\min}$) is already a lower symmetry situation than the Dot case (see Fig. 1), and, in addition, the magnetic field breaks the $\pm m$ degeneracy. The arrows in Fig. 4 identify the first three GS transitions, the level crossing from the $m-1$ to the m state, for $m=1, 2$, and 3 ($n=0$). In the inset we show the celerylike Fock-Darwin spectrum; these levels touch each other at the infinity limit ($b \rightarrow \infty$).

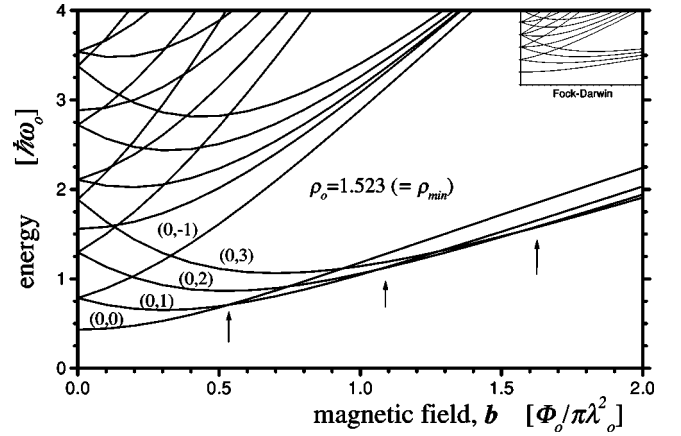


FIG. 4. Lowest lying Hill energy levels versus magnetic field, for a ring with $\rho_o = 1.523 (= \rho_{\min})$. The twofold degeneracy between states with the same value of n and $|m|$ is broken by the magnetic field. The arrows point to the first three level crossing of the GS: from the (0,0) to the (0,1), then to the (0,2), next to the (0,3). The inset shows the Fock-Darwin spectrum. There is no level crossing for the Dot.

In our notation the number of flux quanta threading the inner region of the rings ($\rho \leq \rho_o$) is directly given by $b\rho_o^2 = (B\pi\lambda_o^2/\Phi_o) \times (\rho_o^2/\lambda_o^2) \equiv \Phi_{\rho_o}$.

For an ideal 1D ring (a bent 1D wire) these level crosses occur when $(m-1/2)$ flux quanta are trapped in the ring (dotted line in Fig. 5), the signature of the Bohm-Aharonov¹ effect. These transition points (LCP: level crossing points) are routinely used in experiments to estimate effective radius for the rings, but for 2D rings the exact position of these LCP strongly depend on the size of the ring and the characteristics of the confining potential.⁶

Figure 5 shows that for high values ($\rho_o \gtrsim 5$) the results for both potentials tend to those of the 1D ring. But there are strong differences at lower values of ρ_o : Whereas the Volcano LCP are at lower trapped flux values than the ones of the 1D-ring, the Hill LCP are at greater values of Φ_{ρ_o} . The

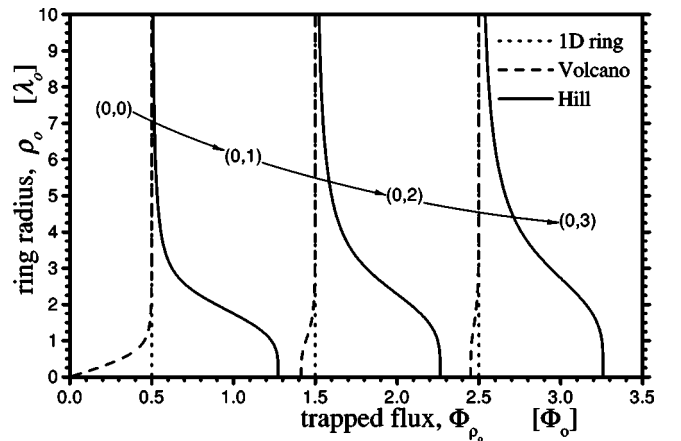


FIG. 5. Trapped magnetic flux (Φ_{ρ_o}) at the first, second, and third GS level crossing for the analyzed potentials, as a function of the ring radius ρ_o . The Hill potential response is softer (Dot like) than the 1D ring, whereas the Volcano one is harder.

Hill GS tolerate higher values of magnetic flux before crossing the following m state.

For the Volcano these LCP, defined by $E_{0,m}^V = E_{0,m-1}^V$, are given by

$$\Phi_{\rho_o}^V(m) = \frac{1}{\sqrt{2}} [m m_- - a + \sqrt{(m^2 + a)(m_-^2 + a)}]^{1/2}, \quad (13)$$

where $m_- = m - 1$, and $a = \rho_o^4$. The dashed lines in Fig. 5 show this result for $m=1, 2$, and 3 . This same equation [Eq. 13] holds for the LCP of the higher energy bands ($n > 0$) of the Volcano potential. The behavior of the Volcano LCP at low values of ρ_o can be traced back to the effect of the “centrifugal-like” repulsive core of this potential: Taking into account the mean radius (weight center) of a Volcano m state given in Ref. 12 ($\rho_m \sim \sqrt{M}$), it can be seen that the energy cost [the $M\sqrt{1+b^2}$ term in Eq. (5)] due to this enlarged mean radius overcomes the orbital Zeeman energy (the $-mb$ term), compared with the corresponding terms in the Fock-Darwin spectrum [Eq. (2)]. This effect is particularly strong for the (0,0) state, which has a finite value for M (but $m=0$), as a consequence the (0,0) to (0,1) LCP line starts at zero trapped flux for this potential.

For the Hill potential these LCP are obtained numerically. The $\rho_o \rightarrow 0$ limit can be analytically discussed. In this limit the ring with a Hill potential can be considered as a weakly perturbed Dot. Application of perturbation theory allows then a straightforward calculation of the energy of the states to first order in ρ_o . The LCP (for the GS, the $n=0$ band) are obtained from the condition $\langle m-1 | H_H | m-1 \rangle_D = \langle m | H_H | m \rangle_D$, which yields

$$\sqrt{1+b^2} = b + \frac{G(m)\rho_o}{(1+b^2)^{1/4}}, \quad (14)$$

where $G(m) = \Gamma(m+1/2)/2m!$. From this equation the trapped flux at the Hill LCP in the limit $\rho_o \rightarrow 0$ ($b \rightarrow \infty$) can be obtained

$$\Phi_{\rho_o \rightarrow 0}^H(m) = \frac{1}{4G^2(m)}. \quad (15)$$

Equation (15) gives $4/\pi$, $64/4\pi$, and $256/25\pi$ (1.273, 2.263, and 3.259) for $m=1, 2$, and 3 , respectively, i.e., the $\rho_o=0$ points of the Hill LCP lines, the full lines in Fig. 5. Note that these Hill LCP points (at $\rho_o=0$) can also be interpreted as Dot LCP; there is no contradiction with the Fock-Darwin spectrum, i.e., the trapped flux is finite, but the applied field diverges as $1/\rho_o^2$. This Dot-likeness of the Hill states at low values of ρ_o is consistent with the analysis of the Hill GS of the previous subsection.

In the rings of Ref. 5 the first LCP point is roughly at $\Phi_{\rho_o} \sim 1$, ($\rho_o \sim 1.5$ for them), favoring the use of the Hill potential (or similar potentials with just a bump at the ring center) over the Volcano in order to model the experimental situation.

C. Rings with broken azimuthal symmetry

Self-assembled rings do not usually have a perfect rotational symmetry. This fact must be taken into account be-

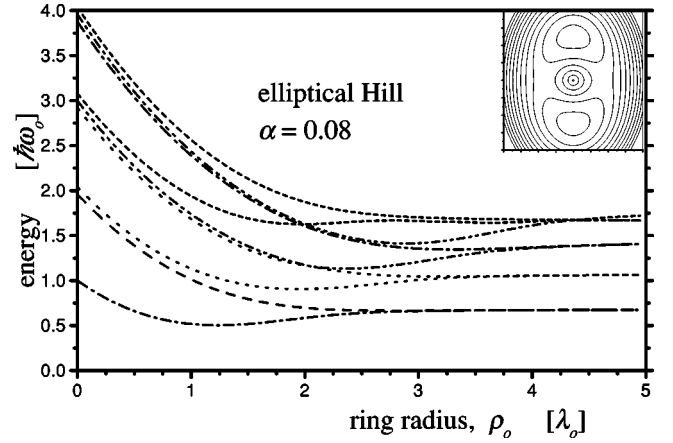


FIG. 6. Lowest lying energy levels of the Hill ring with a small elliptical asymmetry. No degeneracy exists among the energy levels, except in the limit $\rho_o \gg 1$. The inset shows a contour plot of the potential ($\alpha=0.2, \rho_o=4$).

cause what most experiments measure are transitions between different eigenstates under the action of electromagnetic radiation fields, and the selection rules for such transitions strongly depend on which symmetries are present in the samples.

A common experimental situation is the presence in these rings of an elliptical deformation.¹⁶ This lower symmetry is due to the presence of an easy-growth axis in the surface of the substrate over which the rings are formed. The rings are enlarged and thickened in this axis directions. To model this deformation we add the following term to the ring potentials^{17,18}

$$V_2 = \frac{1}{2} \alpha \cos(2\varphi) \rho^2 + C. \quad (16)$$

The overall confining potential (the leading term for $\rho \gg 1$) is given then by $\frac{1}{2}(1 + \alpha \cos 2\varphi)\rho^2$; the C term in Eq. (16) is such that the minimum value of the potential remains at zero, $C = \frac{1}{2}\rho_o^2\alpha/(1-\alpha)$ for the Hill potential.

The matrix elements for this deformation can be easily evaluated in the ladder representation (see Appendix). For the present analysis it is enough to say that this deformation mixes states with angular quantum numbers that differ by two units (there is a $\delta_{m',m\pm 2}$ factor in the elements, which is already apparent in the (ρ, φ) space representation). Therefore parity is preserved, and therefore there is a Hilbert subspace for the odd m 's and another for the even m 's. As radiation assisted transitions usually imply $\Delta m = \pm 1$, in the present case it will involve transitions between these two subspaces. The relative amplitude of these transitions could be traced back because the method provides us with the expansion coefficients of the states in the Dot basis, in which these amplitudes can be easily evaluated, although this is not the purpose of the present study. There is also a $1/\sqrt{1+b^2}$ multiplicative factor in these elements: The magnetic field tends to reduce the relative weight of the deformation, trying to restore the azimuthal symmetry for high values of b .

In Fig. 6 we show the spectrum of a slight deformed Hill

potential at zero magnetic field ($\alpha=0.08$, $b=0$). The rupture of the azimuthal symmetry is apparent, even at $\rho_o=0$. The asymptotic values ($\rho_o \gg 1$) of the lower eigenvalues of the spectrum can be fully accounted for with a “small oscillation” analysis of the confining potential. Instead of the circular valley of the perfect ring (at $\rho=\rho_o$) there are now two kidneylike minima over the y axis [at $y=\pm\rho_o/(1-\alpha)$] and two saddle points over the x axis [at $x=\pm\rho_o/(1+\alpha)$] (see inset in Fig. 6). Expanding the total potential, Eq. (16) plus Eq. (3), around one of these minima one obtains two parabolic “spring constants,” $k_x=2\alpha$ and $k_y=(1-\alpha)$. The corresponding frequencies $\omega_x=\sqrt{2\alpha}$ and $\omega_y=\sqrt{1-\alpha}$ for this harmonic oscillator approximation, plus bonding/antibonding mixtures of the states localized around each of the two minima, fully explain this region of the spectrum and the corresponding wave functions.

Due to the spectrum characteristics discussed above, elliptical deformed self-assembled rings of large ρ_o are possible good “two level” systems to use in quantum computation,¹⁹ easily tunable by means of (in plane) electric¹⁴ or (perpendicular) magnetic fields. The massive number of rings in a given sample⁵ ($\sim 10^8$ rings/mm²) could allow for a “probabilistic” lecture of the results of a quantum computation.

IV. FITTING TO EXPERIMENTAL DATA

Excitation energies ($\varepsilon_{qn}=E_{qn}-E_{GS}$, where qn are the quantum numbers of an excited state) are the relevant numbers in an experimental situation. For electromagnetic radiation assisted transitions, a $|\Delta m|=1$ selection rule is in effect. This limitation holds for perfect circular rings, but is relaxed for deformed ones, given that the m s are no longer strict quantum numbers. Nevertheless, for slight deformations the m label is still a good description of the states for most of the spectrum regions, except for the points at which directly mixed states (for example, $|\Delta m|=2$ for the elliptical deformation) have nearly equal energies. At these points a strong mix of the near degenerated nondeformed states forms the actual eigenstate of the deformed ring.

In Fig. 7 we plot the ratio between the energy of the two first possible transitions at $B=0$, $g=\varepsilon_{1,1}/\varepsilon_{0,1}$, as a function of the ring radius ρ_o , for the Hill and Volcano potentials. This ratio is highly dependent on the radius and also on the degree of deformation of the rings (α). If experimentally available, this ratio allows for the characterization of the ring. Used in conjunction with the first level crossing (LCP) pattern curve (Fig. 5), a useful characterization of an experimental sample can be quickly obtained.

The $\varepsilon_{0,1}$ data is not available for the rings of Ref. 6 (square dots in Fig. 8), but an approximate fitting to the experimental data can be made. On the right of Fig. 8 we reproduce the fitting already given by Emperador *et al.*,⁶ which corresponds to $\hbar\omega_o=13.5$ meV, $\rho_o=14$ nm ($=1.485 \lambda_o$), $\alpha=0$ (and $m_e^*=0.063 m_e$). The dashed lines ($|\Delta m|=3$ or greater) are forbidden transitions for a perfect ring. On the left we present another fitting with slightly different parameters ($\hbar\omega_o=13$ meV, $\rho_o=1.4 \lambda_o$, $\alpha=0.02$). Due to the break of the azimuthal symmetry new transitions are

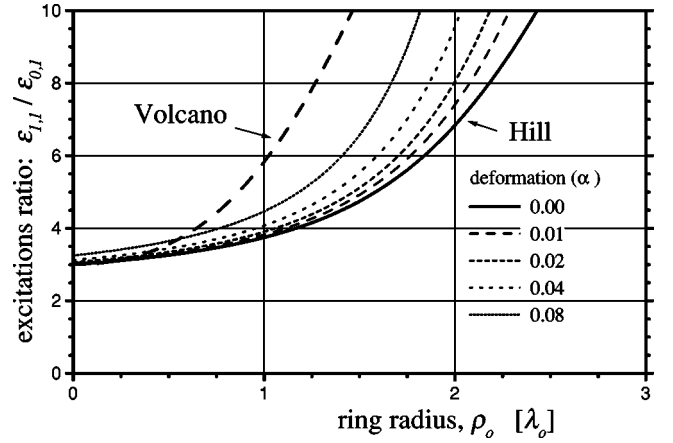


FIG. 7. Excitation ratio ($\varepsilon_{1,1}/\varepsilon_{0,1}$) at $B=0$ for the Hill and Volcano potentials. This ratio depends strongly on the ring size, and can then be used to characterize samples.

now possible, although their intensities are lower than the principal ones. Roughly estimated intensities are represented by linewidth: feeble lines correspond to less probable transitions. Experimental points without explanation on the right side fitting can now be interpreted as less probable excitations, allowed by the symmetry break.

A similar effort to fit the Volcano potential parameters to the same experimental data does not give consistent results. This is essentially due to the results of Fig. 5 above, as for $\rho_o \approx 1.4 \lambda_o$ the first crossing level for the Volcano potential lies at $\Phi_{\rho_o} \approx 0.5$, instead of ≈ 1 , as experimentally observed.

V. CONCLUSIONS

We have thoroughly studied the size, magnetic field, and symmetry dependence of the electronic level structure of

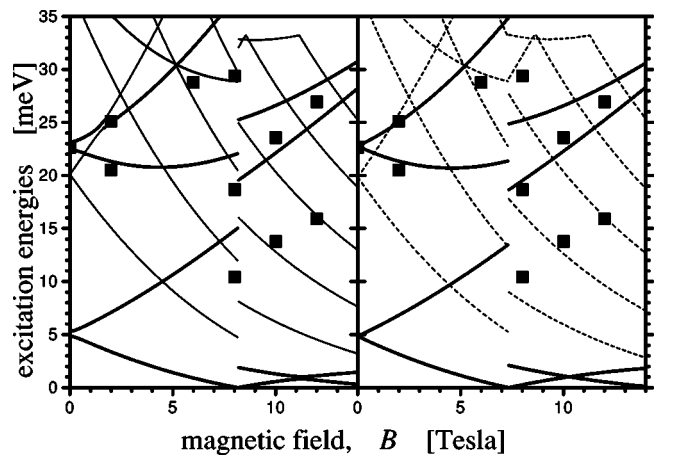


FIG. 8. Hill potential fitting to the experimental data of Ref. 6. On the right there is a “perfect ring” fitting ($\hbar\omega_o=13.5$ meV, $\rho_o=14$ nm, $\alpha=0$), and the dashed lines are forbidden excitations. On the left we use ($\hbar\omega_o=13$ meV, $\rho_o=1.4\lambda_o$, $\alpha=0.02$), i.e., a deformed ring; new excitations are possible (see text). The breaks on the lines of both sides (at $B \sim 8$ T) signals the first GS LCP point for this sample.

semiconductor self-assembled quantum rings, within the single-particle scheme. Two alternatives for the ring lateral confining potential have been considered: one with a centrifugal-like core (Volcano), and the displaced parabola (Hill). While the first admits an analytical solution, the second requires a numerical analysis.

We have found that the lowest energy level of the Hill rings has an absolute minimum as a function of the ring radius, at $\rho_o \approx 1.5 \lambda_o$. This minimum represents an electronic contribution to the energy of formation of these rings, which can help to stabilize rings of this size. Actually, the experimentally available rings have radii in this range. This minimum is not present for the Volcano confinement.

In the presence of a perpendicular magnetic field, the studied confining potentials display strikingly different behaviors. Taking the perfect one-dimensional ring as reference, the ground-state transitions driven by the magnetic field are easier for the Volcano and harder for the Hill potential, with the crossing points lying to the left (smaller fields) and to the right (larger fields) of the 1D ring crossing points, respectively. Experimental crossing points are in quantitative agreement with the Hill result.

The electronic structure of rings with a Hill confinement potential with a weak elliptical deformation have been obtained, and compared with experimental data. From this comparison, we have confirmed that the Hill confinement potential provides a suitable theoretical description of the actual self-assembled rings.

We remark in the Appendix on the existence of phase factors, usually disregarded, between two widely used basis of the parabolic Dot.

ACKNOWLEDGMENTS

J.S. and C.R.P. are fellows of CONICET. This research was partially supported by FONDECYT(Chile) under Grant No. 7020839, and CONICET(Argentina) under Grant No. PIP 02753/00.

APPENDIX: DOT LADDER OPERATORS

The ladder operators are a useful 2D generalization of the well-known number operators of the 1D harmonic oscillator. Different derivations of them can be found in the available literature, but their relation with other representations of the 2D harmonic oscillator is scarcely given. Hence a brief recount is worthwhile. As a recent summary has been given in Ref. 10 (Sec. III C, pp. 17–20, hereafter QDots), we closely follow this presentation of the subject.

After introducing the complex variables $u=x+iy$ and $v=x-iy$, the boson ladder creation operators for the harmonic 2D Dot are defined as [QDots (3.9) to (3.11)]

$$a^\dagger = \frac{1}{2}(u - 2\partial_v), \quad b^\dagger = \frac{1}{2}(v - 2\partial_u), \quad (\text{A1})$$

where lengths are normalized by λ_ω (QDots l_0 is equal to $\lambda_\omega/\sqrt{2}$). In the basis expanded by these operators the eigenstates of the Fock-Darwin Hamiltonian are given by [QDots (3.17)]

$$|n_a, n_b\rangle = \frac{1}{\sqrt{n_a! n_b!}} (a^\dagger)^{n_a} (b^\dagger)^{n_b} |0, 0\rangle, \quad (\text{A2})$$

the quantum number n_a (n_b) in this representation indicates the number of a (b) excitations in the state, and $|0, 0\rangle$ is the vacuum state. The following expression for these states as a function of u, v is given in QDots [QDots (3.20)]

$$\Phi_{n_a, n_b} = \frac{e^{uv/2}}{\sqrt{\pi}} \frac{1}{\sqrt{n_a! n_b!}} (\partial_u)^{n_b} (\partial_v)^{n_a} e^{-uv}. \quad (\text{A3})$$

For the (ρ, φ) representation QDots use the same expression than we do, Eq. (1) [QDots (3.21) to (3.24)], QDots n_r is our n . We will also need the Laguerre polynomials definition

$$L_n^{|m|}(w) = w^{-|m|} \frac{e^w}{n!} \frac{d^n}{dw^n} (w^{n+|m|} e^{-w}). \quad (\text{A4})$$

The relation among the quantum numbers of these two representations is $n = \min(n_a, n_b)$, and $m = n_a - n_b$.

These results, however, should be used with great care, as important phase factors are missing between the $|n_a, n_b\rangle$ and the $|n, m\rangle$ relations given above.

One missing phase factor is between the $|n_a, n_b\rangle$ states and their u, v representation [Eqs. (A2) and (A3)]. Applying the a^\dagger rising operator to Φ_{n_a, n_b} one obtains

$$\begin{aligned} \frac{1}{2}(u - 2\partial_v)\Phi_{n_a, n_b} &= \frac{u}{2}\Phi_{n_a, n_b} \\ &\quad - \partial_v \left[\frac{e^{uv/2}}{\sqrt{\pi}} \frac{1}{\sqrt{n_a! n_b!}} (\partial_u)^{n_b} (\partial_v)^{n_a} e^{-uv} \right] \\ &= \frac{u}{2}\Phi_{n_a, n_b} - \frac{u}{2}\Phi_{n_a, n_b} \\ &\quad - \frac{e^{uv/2}}{\sqrt{\pi}} \frac{1}{\sqrt{n_a! n_b!}} \partial_v [(\partial_u)^{n_b} (\partial_v)^{n_a} e^{-uv}] \\ &= -\sqrt{n_a + 1} \Phi_{n_a + 1, n_b}, \end{aligned} \quad (\text{A5})$$

i.e., a^\dagger does what a boson creation operator is supposed to do except for a minus factor. Hence, a $(-1)^{n_a + n_b}$ phase factor must be included in Eq. (A3).

Other missing phase factor appears between the $|n_a, n_b\rangle$ states and the $|n, m\rangle$ ones. This one can be found by looking at Eqs. (A3) and (A4). The highest w power term in the Laguerre polynomial comes from the d/dw operator acting always on the e^{-w} exponential factor in the ‘‘nucleus,’’ thus its sign is given by $(-1)^n$. The corresponding term in Φ_{n_a, n_b} comes also from the partial derivatives acting directly on the e^{-uv} exponential nucleus, this gives a $(-1)^{n_a + n_b}$ factor. Hence there is a $(-1)^{\max(n_a, n_b)}$ factor between Eq. (1) and Eq. (A3), and

$$|n_a, n_b\rangle = (-1)^n |n, m\rangle \quad (\text{A6})$$

is then obtained for the relation between these representations (our n , QDots n_r).

These phase factors do not show up if one is working always within a given representation, but they must be carefully taken into account if one wants to make use of the

different representations to evaluate more easily a given matrix element, or if one changes the representation to discuss some point of a given problem (e.g., plot the radial distribution of a wave function evaluated in the $|n_a, n_b\rangle$ representation).

Finally, we present the ladder operators we use. We define the complex variables as

$$u = \frac{1}{\sqrt{2}}(x + iy), \quad v = \frac{1}{\sqrt{2}}(x - iy);$$

$$\partial_u = \frac{1}{\sqrt{2}}(\partial_x - i\partial_y), \quad \partial_v = \frac{1}{\sqrt{2}}(\partial_x + i\partial_y), \quad (\text{A7})$$

where u, v and x, y are in units of λ_ω , the scaling length of the orbitals [see Eq. (1)]. This “normalized” ($1/\sqrt{2}$) definition of u and v avoids the “floating” factors of 2, typical of other possible choices. Both in the new definitions and in the reverse transformations only the factor $1/\sqrt{2}$ appears. The ladder operators become

$$a = \frac{1}{\sqrt{2}}(v + \partial_u), \quad a^\dagger = \frac{1}{\sqrt{2}}(u - \partial_v),$$

$$b = \frac{1}{\sqrt{2}}(u + \partial_v), \quad b^\dagger = \frac{1}{\sqrt{2}}(v - \partial_u). \quad (\text{A8})$$

Note that, using Eq. (A7)

$$a = \frac{1}{2}[(x - iy) + (\partial_x - i\partial_y)]$$

$$= \frac{1}{2}[(x + \partial_x) - i(y + \partial_y)] = \frac{1}{\sqrt{2}}(a_x - ia_y),$$

$$b = \frac{1}{\sqrt{2}}(a_x + ia_y), \quad (\text{A9})$$

where a_x, a_y are 1D boson operators of the harmonic oscillator, one defined for the x coordinate and the other for the y . This holds for any initial definition of u, v , i.e., it also holds for the operators defined in Eq. (A1).

The expression for the $|n_a, n_b\rangle$ states in terms of u, v is given now by

$$\Phi_{n_a, n_b} = \frac{1}{\sqrt{\pi\lambda_\omega}} \frac{(-1)^{n_a+n_b} e^{uv}}{\sqrt{2^{n_a+n_b} n_a! n_b!}} (\partial_u)^{n_b} (\partial_v)^{n_a} e^{-2uv}. \quad (\text{A10})$$

To give an example of the utility of these operators, look that the matrix elements of the elliptical deformation Eq. (16) can be easily evaluated in the ladder representation, given that

$$\rho^2 \cos(2\varphi) = \left(\frac{\lambda_\omega}{\lambda_o}\right)^2 (u^2 + v^2)$$

$$= \frac{1}{2} \left(\frac{\lambda_\omega}{\lambda_o}\right)^2 [(a^\dagger + b)^2 + (a + b^\dagger)^2],$$

the $(\lambda_\omega/\lambda_o)$ factor comes from the fact that lengths in the Hamiltonian are in units of λ_o (a constant for a given ring) whereas the orbitals, and u, v , scale with λ_ω , i.e., they automatically include the effect of the magnetic field on the parabolic confining potential of the Dot. The operator terms in the brackets are evaluated straightforwardly in the $|n_a, n_b\rangle$ representation, given a $\delta_{m', m \pm 2}$ factor when translated to the $|n, m\rangle$ representation, and also strong constraints on the allowed n', n values. This last restriction is not evident if one computes these matrix elements directly in the $|n, m\rangle$ representation.

¹Y. Aharonov and D. Bohm, Phys. Rev. **115**, 485 (1939).

²S. Washburn and R. Webb, Rep. Prog. Phys. **55**, 1311 (1992).

³A. Fuhrer, S. Luscher, T. Ihn, T. Heinzel, K. Ensslin, W. Wegscheider, and M. Bichler, Nature (London) **413**, 822 (2001).

⁴U. Keyser, S. Borck, R. Haug, M. Bichler, G. Abstreiter, and W. Wegscheider, Semicond. Sci. Technol. **17**, 122 (2002).

⁵A. Lorke, R. Luyken, A. Govorov, J. Kotthaus, J. Garcia, and P. Petroff, Phys. Rev. Lett. **84**, 2223 (2000).

⁶A. Emperador, M. Pi, M. Barranco, and A. Lorke, Phys. Rev. B **62**, 4573 (2000).

⁷T. Chakraborty and P. Pietilainen, Phys. Rev. B **50**, 8460 (1994).

⁸V. Fock, Z. Phys. **47**, 446 (1928).

⁹C. Darwin, Proc. Cambridge Philos. Soc. **27**, 86 (1930).

¹⁰L. Jacak, P. Hawrylak and A. Wójs, *Quantum Dots* (Springer, Berlin, 1997).

¹¹J. Kyriakidis, M. Pioro-Ladriere, M. Ciorga, A. Sachrajda, and P. Hawrylak, Phys. Rev. B **66**, 035320 (2002).

¹²W.-C. Tan and J. Inkson, Semicond. Sci. Technol. **11**, 1635 (1996).

¹³W.-C. Tan and J. Inkson, Phys. Rev. B **60**, 5626 (1999).

¹⁴Z. Bartecevic, G. Fuster, and M. Pacheco, Phys. Rev. B **65**, 193307 (2002).

¹⁵If this effect is to be included in a study of the dynamics of ring formation, one must also take into account that the characteristic frequency ($\hbar\omega_o$) will probably depend on the size of the ring, given the constant volume constraint, equal to the starting dot volume.

¹⁶T. Raz, D. Ritter, and G. Bahir, Appl. Phys. Lett. **82**, 1706 (2003).

¹⁷G. Vasile, V. Gudmundsson, and A. Manolescu, in *Physics of Semiconductors 2002*, edited by A. R. Long and J. H. Davies, (IOP, Bristol-Philadelphia, 2003), Vol. 171, pp. A-11.

¹⁸I. Magúsdóttir and V. Gudmundsson, Phys. Rev. B **60**, 16591 (1999).

¹⁹*Semiconductor Spintronics and Quantum Computation*, edited by D. D. Awschalom, D. Loss, and N. Samarth (Springer, Berlin, 2002).